OPEN ACCESS

sensors

ISSN 1424-8220

www.mdpi.com/journal/sensors

Supplementary Information

Sensitivity Comparison of Vapor Trace Detection of Explosives Based on Chemo-Mechanical Sensing with Optical Detection and Capacitive Sensing with Electronic Detection. *Sensors* 2014, *14*, 11467-11491

Drago Strle [1,*], Bogdan Štefane [2], Erik Zupanič [3], Mario Trifkovič [1], Marijan Maček [1], Gregor Jakša [2], Ivan Kvasič [3] and Igor Muševič [3]

[1] Faculty for Electrical Engineering, University of Ljubljana, Tržaška 25, Ljubljana 1000, Slovenia; E-Mails: mario.trifkovic@fe.uni-lj.si (M.T.); marijan.macek@fe.uni-lj.si (M.M.)

[2] Faculty for Chemistry and Chemical Technology, University of Ljubljana, Aškerčeva 5, Ljubljana 1000, Slovenia; E-Mails: bogdan.stefane@fkkt.uni-lj.si (B.Š.); gregor.jaksa@ijs.si (G.J.)

[3] Institute Jozef Stefan, Jamova 39, Ljubljana 1000, Slovenia; E-Mails: erik.zupanic@ijs.si (E.Z.); ivan.kvasic@ijs.si (I.K.); igor.musevic@ijs.si (I.M.)

* Author to whom correspondence should be addressed; E-Mail: drago.strle@fe.uni-lj.si; Tel.: +386-1-4768-847.

S1. Capacitive Sensing with Electronic Detection

S1.1. Architecture of Electronic Detection System

Figure S1 shows a simplified block diagram of a signal processing electronics implemented in 0.25 µm Bipolar, CMOS, Double diffused Metal Oxide Semiconductor (BCD) process. The whole system architecture is a modified lock-in amplifier and consists of: low noise analog electronics, which is currently implemented on the Application Specific Integrated Circuit (ASIC) and the Digital Signal Processing (DSP), which is implemented on the Field Programmable Gate Array (FPGA). In future solutions, this could be integrated on one silicon chip. One channel can, in principle, process the signals from many sensors (only four sensors per measurement channel are used at the moment). Each sensor is surface-functionalised using different chemical modification layers and in this way, they show different sensitivity to the target and other molecules in the atmosphere around the sensors. Using this method and complex signal processing algorithms, chemical selectivity can be improved. Currently, four differently modified sensors are connected to one measurement channel. This number could be increased by connecting more differential sensors to one charge amplifier, while each sensor must be in this case excited with a different excitation signal frequency (see Subsection S1.2.).

The sensor capacitances are driven with differential square-wave signals with adjustable frequency f_{Sx} and amplitude V_{Sx}, resulting in a quasi-square-wave voltage at the output of a charge amplifier with the amplitude of the first harmonic: $V_{\mathrm{Chox}} \cong V_{Sx}(\Delta C_x / C_f)$ at corresponding frequency f_{Sx}. The amplitude of the signal for one sensor is proportional to the difference of the sensor capacitances $\Delta C_x = C_{px} - C_{nx}$ and to the amplitude of the excitation sensor signal V_{Sx}. It is inversely proportional to the feedback capacitor of the charge amplifier C_f. A similar translation happens for each capacitive differential sensor pair at the different excitation frequency $f_{Sx}(x = 1,2,...)$.

Figure S1. Signal processing block diagram of the low noise electronic measurement system that can process signals from four differently modified sensors.

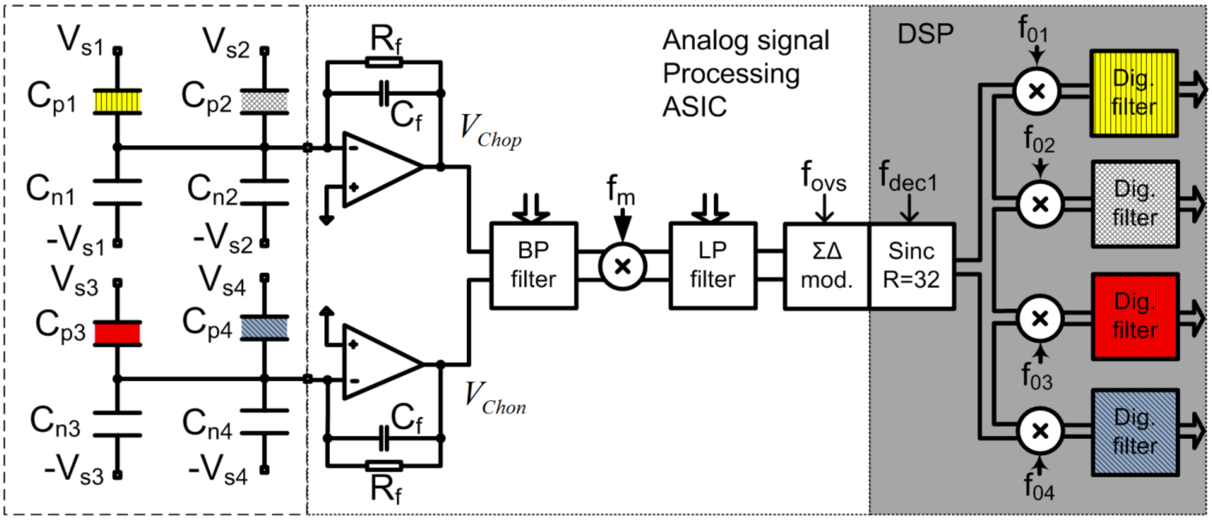

The signal at the output of the charge amplifier V_{Cho} includes information on the capacitance differences of all sensors; each sensor response appears at a different frequency. The complete signal is amplified using a fully-differential and programmable low-noise band-pass amplifier [1]. The resultant signal level is well above the thermal noise level of the following blocks. The composed and amplified signal is mixed with a square-wave signal with frequency f_m in a precision passive mixer [2]. The phase of the mixing signal is digitally adjusted in such a way that the phase difference between the first harmonic of mixing signal and first harmonic of the signal from the band-pass filter is as close to zero as possible. Generally, to measure the impedance, one would need quadrature signal processing; fortunately, in this case we expect only a change in the capacitance of the sensor, whereas the resistive current in the sensor is negligible. After the passive mixer, the resultant spectrum is a composition of sums and differences of all fundamental spectral components and their odd order harmonics. The important spectral components are located at the difference of the first harmonics $f_{ox} = S_{Sx} - f_m$ (x = 1, 2, 3 or 4; see subsection S1.2. for details). The amplitude of the corresponding spectral components is proportional to the excitation signal amplitude (assumed to be constant during the measurements) and corresponding capacitance difference of the sensor, which is caused by the adsorbed target molecules onto the modified capacitor. The low frequency spectral components are amplified, while other components are attenuated using a fourth order, continuous-time low-pass filter with programmable gain and pole frequency that attenuates unwanted high frequency remains at the output of the mixer. The signal levels of the spectral components carrying the information are well above the quantization and thermal noise level of the Σ−Δ Analog to Digital Converter (ADC), while remaining higher harmonics fall outside the band of interest in the band of noise shaped quantization noise; these unwanted components are attenuated with a digital decimation filter implemented in the DSP. A complete analog signal is converted to a digital signal using 18 bits oversampled Σ−Δ AD converter. Further signal processing is digital and consists of digital mixers and Low-Pass (LP) digital filters. Digital mixers translate the signals from $f_{ox}(x = 1,2,\ldots,4)$ down to DC in a four separate digital channels; the phase of each digital mixer signal is again adjusted in such a way that each resulting DC signal has the maximal possible amplitude. The remaining spectral components in each digital channel are located at higher frequencies and are further attenuated in digital low-pass filters, which further reduce the bandwidth. The DSP output rate is approximately 14 samples per second with the word-length of 32 bits. The results are transferred to the personal computer (PC) via USB interface, where further signal processing (averaging), storage and presentation are taking place.

S1.2. Generation of Excitation Sensor Signals

Excitation sensor signals are generated in the FPGA and transferred to the ASIC, where further shaping and amplification takes place. The amplitudes and the DC levels of each excitation signal can be adjusted. They are connected to the corresponding sensor's capacitors and provide the possibility of transferring the information from slowly varying sensor capacitances to the trans-impedance charge amplifier at a high frequency, well above the flicker noise corner frequency. The whole measurement system looks like a modified lock-in amplifier [3,4], using double-mixing architecture to sense and amplify at high frequency above the 1/*f* noise corner of the Complementary Metal Oxide Semiconductor (CMOS) charge amplifier. Once the composite signal amplitude is big enough, the frequency is reduced by down-mixing and thus the power consumption of the remaining modules in the measurement channel is reduced. Each spectral component is not immediately reduced to the DC because, in that case, the 1/*f* noise and the offset voltage of the ADC would influence the results. The other possibility would be to use chopping in each module that constitutes a measurement path (charge amplifiers, Band-Pass (BP) filter, mixer, LP filter, Σ−Δ modulator) and use a DC excitation signal. However, in that case, the noise penalty would be higher and thus the overall sensitivity would be worse compared to the suggested architecture. The amplitudes, DC levels, and frequencies of excitation signals are programmable, and we can adapt each excitation generator to a particular sensor. At the moment up to four differential sensors are connected to one measurement channel according to Figure S1. Each sensor is driven by a square-wave excitation signal with slightly different frequency f_{sx} Two single-ended charge amplifiers, instead of a single fully differential charge amplifier are used to keep the potential of one sensor's node at fixed (programmable) virtual ground potential V_g. Each measurement channel contains two charge amplifiers; each amplifier processes the signals from two differential sensors, therefore, one measurement channel can process the signals of four differential sensors.

The circuit must be as simple as possible, and the influence of jitter must be minimized not to influence the *S*/*N* of a sampled data system. All signals are derived from one master clock with a frequency f_{clk} = 25 MHz using programmable dividers. The frequencies are adjusted in such a way that the signals are coherent [5]. One possible selection of important signal frequencies for four sensors per channel might be: f_{ovs} = 6.25 MHz (oversampling frequency of a $\sum-\Delta$ modulator), $f_{dec1} = f_{ovs}/16$ = 390.6 kHz (output sampling frequency of the first decimator), $f_{\mathrm{m}} \cong 195.3$ kHz (analog mixing frequency), $f_{Sx} \cong \{204.03, 206.45, 208.99, 211.66\}$ kHz (sensor excitation signal frequencies), $f_{\mathrm{dec2}} = 1.5$ kHz (output sampling frequency of the second decimation filter), $f_{ox} \cong \{8.8, 10.9, 13.9, 16.3\}$ kHz (digital mixers frequencies), and $f_{\mathrm{dec3}} = 11.9$ Hz (sampling frequency of the third decimation filter). High frequencies f_{Sx} of excitation signals makes it possible to sense slowly changing capacitance difference at a frequency well above the $1/f$ noise corner of the analog electronics, while preserving all fluctuations of the sensors' capacitances, even those at DC. The "DC" signal processing happens only in the DSP, and thus all DC drifts and $1/f$ noise problems of the analogue electronic modules are removed. As a result, the noise properties are improved. The coherence of all important signals in the measurement system is maintained in an efficient way by keeping the ratio of f_{dec1}/f_{ox} as an even integer.

S1.3. Calibration

Matching properties of the sensors and additional modification monolayer on one capacitor may cause the initial capacitance differences of up to 10%, which would drive the measurement channel into saturation at high gain, which is needed for the required sensitivity. This would limit possible amplification in the channel, and also limit the amplitude of each excitation signal and thus reduce the sensitivity. Programmable capacitors are therefore implemented on the chip; they are connected in parallel to each sensor's capacitor and have a value from 1 fF up to approximately 64 fF in steps of 1 fF. In future, the resolution and the range will be increased. During calibration in a neutral atmosphere, the capacitance difference of each differential sensor is measured, the results are stored, and the total capacitance difference for each sensor is brought close to zero. The initial signal amplitude in the measurement path is reduced; the gain in the measurement channel and excitation signal amplitudes can be increased. This procedure is especially important if more sensors are connected to one measurement channel because in this case, many spectral components are present in the measurement channel at the same time, and the intrinsic signal in the channel can be very big. The spectrum at the output of the analogue measurement path for four different sensors is presented in Figure S3; the capacitance of each sensor is calibrated to the capacitance difference shown on that figure.

S1.4. Sensitivity and Noise Considerations

Figure S2 shows a simplified electrical scheme of one charge amplifier. It consists of a high gain, single-ended, folded cascade low-noise operational amplifier with feedback impedance formed by parallel connection of C_f and R_f. The time constant is selected in such a way that the S/N at the output is optimal. Since the optimum S/N is dictated by the sensor and the feedback capacitance and the pole frequency formed by $C_f\,R_f$ must be as low as possible, the resistance is very high, *i.e.*, in a range of several tens of $\mathrm{G}\Omega$. The R_f is implemented as an active resistor according to [6]; One charge amplifier processes charges from two differential sensors that are driven by excitation signals (V_{S1p}, V_{S1n}) and (V_{S2p}, V_{S2n}) with different frequencies. The model for sensitivity calculations includes:

- A simplified model of the sensors, each presented as a pair of capacitors (C_{p1}, C_{n1}) and (C_{p2}, C_{n2}); differently functionalised capacitors are highlighted by different colours
- Most important parasitic capacitances C_{parASIC}, C_{par} and $C_{\mathrm{parS1}p}$ to $C_{\mathrm{parS2}n}$

- Most important noise sources marked in blue on Figure S2 are: V_{ndop}, V_{ndBp}, V_{ndRf} and V_{ndS1p} through V_{ndS2n}

Figure S2. Simplified electrical diagram of one charge amplifier with two differential sensors, parasitic capacitances, and the most important noise sources.

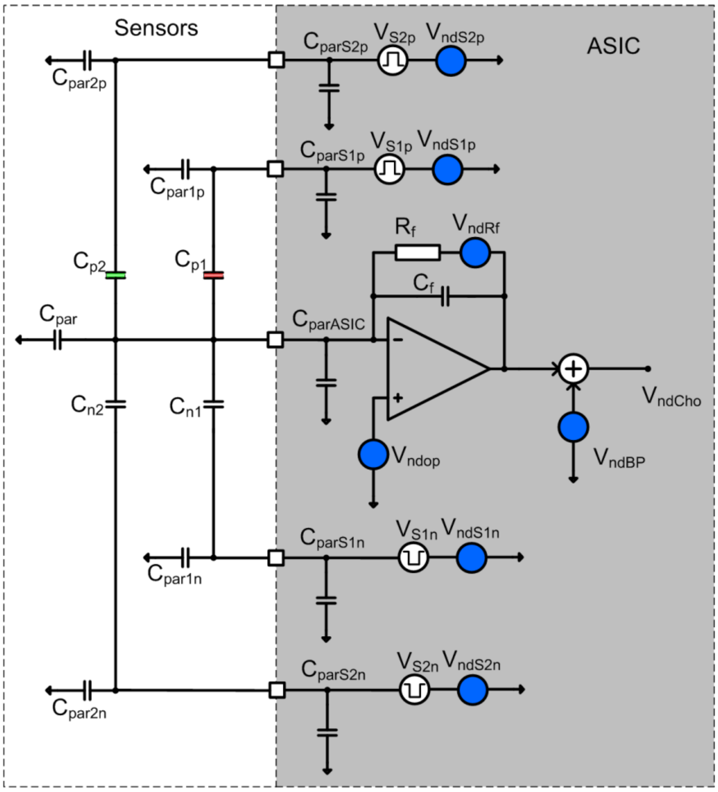

The Circuit diagram shown on Figure S2 is used for detector-sensitivity estimation. The decisive parameter regarding the detection sensitivity of a measurement system is the signal to noise ratio at the output of the charge amplifier (S1) in 1 Hz bandwidth around the corresponding spectral line. Assuming that other modules in the measurement channel contribute a negligible amount of noise, one can estimate the S/N at the output of a charge amplifier using Equation (S1) where V_{Cho} is the amplitude of the corresponding spectral line from the sensor, which can be calculated using Equation (S2), while V_{ndCho} is a noise density at the output of a charge amplifier including an input referred noise density from the following BP amplifier stage; it can be estimated using Equation (S3):

$$\left(\frac{S}{N}\right) \cong \frac{V_{\mathrm{Cho}}}{\sqrt{2} \cdot V_{\mathrm{ndCho}}} \tag{S1}$$

$$V_{\mathrm{Chox}}(\omega) \cong V_{Sx} \frac{\Delta C_x}{C_f} H_{\mathrm{CHA}}(\omega) \tag{S2}$$

The meaning of the symbols in Equation (S2) are the following: $V_{\mathrm{Chox}}(\omega)$ is the amplitude of the spectral component of sensor x at the output of the charge amplifier as a function of frequency, V_{sx} is the amplitude of the corresponding excitation signal, $\Delta C_x = C_{px} - C_{nx}$ is the capacitance difference between the capacitors of the sensor with index x, C_f is the feedback capacitor of the charge amplifier, and $H_{\mathrm{CHA}}(s) \cong s/(s+\omega_p)$ is the High–Pass (HP) signal transfer function, which shapes the excitation signal through the sensor to the output of the charge amplifier with a pole frequency determined by $\omega_p = 1/\left(R_f C_f\right)$. For appropriately selected element values of the charge amplifier and appropriate excitation sensor signal frequency, the absolute value of the transfer function at the excitation frequency is $\left|H_{\mathrm{CHA}}\left(\omega_x\right)\right| \cong 1$, because the excitation sensor signal frequencies are well above the pole frequency ω_p of the charge amplifier. For proper operation of a charge amplifier, which processes more than one sensor signal, it is essential that the initial sensor's capacitance difference is reduced for each sensor using the calibration protocol as explained in subsection S1.3.

The total noise power density at the output of the charge amplifier can be calculated using Equation (S3) and assuming that the noise sources are uncorrelated. If designed properly, the main noise contributor is V_{ndop} multiplied by $\left(1+\sum C_{\mathrm{VG}}/C_f\right)$, where C_{VG} is the sum of all capacitors connected to the virtual ground of the charge amplifier including all parasitic capacitances. The corresponding noise transfer functions and their approximate absolute values can be calculated using Equation (S4) for op-amp noise, Equation (S5) for the excitation signal generators, and Equation (S6) for the feedback resistor contributions. V_{ndBP}^2 in Equation (S3) is the noise contribution of the following BP amplifier and represents the input referred noise of all following stages in the measurement channel, including the noise increase due to analog and digital mixing; their contributions are negligible, because they are located after the gain stage:

$$V_{\mathrm{ndCho}}^2 \cong \left[V_{\mathrm{ndop}}\left|H_{\mathrm{NCho}}(\omega)\right|\right]^2 + V_{\mathrm{ndBP}}^2 + 4\left[V_{\mathrm{ndSx}}\left|H_{\mathrm{NS}}(\omega)\right|\right]^2 + \left[V_{\mathrm{ndRf}}\left|H_{\mathrm{Rf}}(\omega)\right|\right]^2 \tag{S3}$$

$$\begin{gathered} H_{\mathrm{NCho}}(s) \cong \left(1+\frac{\sum C_{\mathrm{VG}}}{C_f}\right)\frac{s+\omega_z}{s+\omega_p}; \quad \omega_z = \frac{1}{R_f\left(C_f+\sum C_{\mathrm{VG}}\right)}; \quad \omega_p = \frac{1}{R_f C_f}; \\ H_{\mathrm{NCho}}(\omega_x) \cong \left(1+\frac{\sum C_{\mathrm{VG}}}{C_f}\right) \quad \text{for} \quad \omega_x > \omega_p > \omega_z \end{gathered} \tag{S4}$$

$$H_{\mathrm{NS}}(s) \cong \frac{C_{Sx}}{C_f}\frac{s}{s+\omega_p}; \quad \left|H_{\mathrm{NS}}(\omega_x)\right| \cong \frac{C_{Sx}}{C_f} \quad \text{for } \omega_x > \omega_p \tag{S5}$$

$$H_{Rf}(s) \cong \frac{\omega_p}{s+\omega_p}; \quad \left|H_{Rf}(\omega_x)\right| \cong \frac{\omega_p}{\omega_x} \quad \text{for } \omega_x > \omega_p \tag{S6}$$

The major contributor to the output noise power is the opamp noise multiplied by $\left(1+\sum C_{\mathrm{VG}}/C_f\right)$. A careful design of the op-amp is therefore necessary by minimizing the op-amp noise V_{ndop} as much as possible. In addition, careful design of the ASIC and the sensor pair is necessary in order to reduce the factor $\left(1+\sum C_{\mathrm{VG}}/C_f\right)$. The noise power contributions from the excitation signal generator is handled easier because the sensor's capacitors C_{Sp} and C_{Sn} are smaller than the feedback capacitor C_f The contribution of one generator is multiplied by 4 because of 4 sensors connected to the charge amplifier; in addition it is not difficult to build low noise excitation generators. The last term in Equation (S3) is due to the feedback resistor R_f. The contribution is small, if the resistance R_f is sufficiently high. This contradicting conclusion can be deduced from the following considerations: the thermal noise power density of the resistor is $V_{\mathrm{ndRf}}^2 \cong 4kTR_f$, so it is proportional to the resistance and the temperature. On the other hand, the noise transfer function $\left|H_{Rf}\left(\omega_{sx}\right)\right|^2 \cong \left(\omega_p / \omega_x\right)^2$ attenuates the noise power around the excitation signal frequency ω_x considerably if $\omega_x > \omega_p$; the slope is −40 dB per decade for the noise power. While the noise power density of the resistor increases linearly with the resistance, the attenuation of the noise transfer function increases with a quadratic law, so the noise at the output decreases linearly with increasing resistance R_f. Its contribution to the noise in the measurement channel is negligible, if $\omega_x > \omega_p$. For more than one differential sensor connected to a single charge amplifier, the required signal range of the amplifier increases because of more spectral components; the amplitude of each spectral component remains the same, whereas the noise density increases because $\sum C_{\mathrm{VG}}$ becomes bigger, therefore very careful design optimization is needed to not increase the noise.

Assuming that V_{ndRf} and V_{ndSx} contribute approximately the same noise power through their noise transfer functions as the op-amp, and that V_{ndBP} (it is input referred noise density of all following signal processing stages) contributes the same amount of noise power, then the total noise power density at the output of the charge amplifier can be estimated: $V_{\mathrm{ndCho}}^2 \cong 3\left[V_{\mathrm{ndop}}\left(1+\sum C_{\mathrm{VG}} / C_f\right)\right]^2$. From these considerations, the S/N at the output of the charge amplifier is estimated using Equation (S7):

$$\left(\frac{S}{N}\right) \cong \frac{S_{Sx}\dfrac{\delta C_x}{\sqrt{2}C_f}}{\sqrt{3}\left[V_{\mathrm{ndop}}\left(1+\dfrac{\sum C_{\mathrm{VG}}}{C_f}\right)\right]} = \frac{V_{Sx}\cdot\delta C_x}{\sqrt{6}\cdot V_{\mathrm{ndop}}\left(C_f+\sum C_{\mathrm{VG}}\right)} \tag{S7}$$

The minimum detectable capacitance difference of sensor x can be calculated using Equation (S8), taking into consideration that the signal power must be at least three times as large as the noise power in the specified band. The charge amplifier is designed with the following parameters: $V_{\mathrm{ndop}}\left(\omega_x\right) \le 7.5\ \mathrm{nV}/\sqrt{\mathrm{Hz}}$, $V_{Sx} = 5\ \mathrm{V}$, $C_f = 2\ \mathrm{pF}$ and $\sum C_{\mathrm{VG}} = 2\ \mathrm{pF}$. The factor $\sqrt{2}$ in the right part of Equation (S7) and in Equation (S8) takes into considerations all contributions, including the amplitude to rms conversion for the first harmonics, and the fact that a detectable signal must have at least 3 times higher signal power than the noise in the specified band. The reduction of the S/N ratio caused by analog and digital mixers is negligible, because each mixing contributes approximately $\sqrt{2}$, if designed properly [7,8]. In reality, the only significant contribution to the V_{ndBP} is the input referred noise of the BP amplifier. With a careful design of all elements, including the sensor, it is possible to improve the detection level of δC even further:

$$\delta C \cong 3\sqrt{2}\frac{V_{\mathrm{ndop}}}{V_{Sx}}\left(C_f+\sum C_{\mathrm{VG}}\right) \cong 4.5\cdot 10^{-20}\left[\frac{F}{\sqrt{\mathrm{Hz}}}\right] \tag{S8}$$

For a comb capacitive sensor with the separation between two comb fingers of $d_0 \cong 1\ \mu\mathrm{m}$, and the initial capacitance of approx. $C_0 = 0.5\ \mathrm{pF}$, it is possible to estimate the minimum detectable separation change in plates δ_{m} between two comb fingers due to the adsorption according to Equation (S9). The following assumptions were taken into consideration for this approximation: (a) the adsorbed molecules only change the separation between the two capacitor plates and not the dielectric constant of modified capacitors significantly (this is an approximation valid if the dielectric constant of adsorbed target molecules is much bigger than the dielectric constant of the air), (b) the surface of the comb capacitor is completely covered with the modification layer, (c) the adsorbed molecules cover the modification layer uniformly and completely, (d) the minimum detectable capacitance of the electronic measurement system can be calculated using Equation (S8). The estimated detectable separation change according to Equation (S9) is approximately 80 fm, which is well below the thickness of one layer of adsorbed target molecules estimated to 0.5 nm [9] for TNT. This fact can be used to measure the density of target molecules (for now TNT) in the atmosphere around the sensor. The fact that δ_m is much smaller than the size of the target molecule makes the measurements possible even if the comb capacitor surface is not covered completely and the density of target molecules is smaller than the number of target molecules at vapour pressure:

$$\delta_m \cong \frac{d_0 \cdot \delta C}{\left(C_0 + \delta C\right)} \cong 8 \times 10^{-14}\ m \qquad \text{(S9)}$$

S1.5. System Level Verification

To verify the concept, sensitivity, and functionality, the sensors and the whole electronic measurement system were modelled on a high hierarchical level using Matlab/Simulink; the most important non-ideal effects of the IC analog measurement path were taken into consideration (such as the nonlinearities, thermal noise, flicker noise, *kT*/*C* noise, spread of elements, offset voltages, *etc.*) [10] and a bit-true model of the complete DSP part was used [11]. The system level simulation results are very close to the estimates, to the circuit simulation results, and to the measurements of the real circuit. Figure S3 shows the spectrum at the output of the Analog Front-End (AFE) for four sensor elements that are driven with excitation signals with different frequencies: $f_{Sx} \cong \{204.03,\ 206.45,\ 208.99,\ 211.66\}\ \text{kHz}$ and amplitude of $V_S = 5\ \text{V}$. The sensors are modelled as capacitors with different capacitances: $\delta C_1 = 100\ \text{aF}$, $\delta C_2 = 50\ \text{aF}$, $\delta C_3 = 10\ \text{aF}$, $\delta C_4 = 5\ \text{aF}$. The model includes the effects of the most important parasitic capacitances. The high frequency spectrum is translated to a lower frequency in an analog mixer, the resulting spectrum is LP filtered and converted to digital stream. Figure S3 shows the simulated spectrum at the output of the $\sum\Delta$ modulator. The spectrum is composed of four main spectral lines at frequencies $f_{ox} \cong \{8.8, 10.9, 13.9, 16.3\}\ \text{kHz}$ with different amplitudes, which correspond to different sensors. The sensitivity is better than 0.04 $\text{aF}/\sqrt{\text{Hz}}$, which is very close to the estimate given in Equation (S8). Higher frequency components are attenuated in a digital decimation filter, currently implemented on the FPGA. The signal to noise ratio (SNR1 on Figure S3) is calculated for the first spectral line around 10 kHz with a 200 Hz bandwidth; from this result one can calculate the sensitivities normalized to the 1 Hz band shown on Figure S3.

It is possible to improve the sensitivity of the sensor and the measurement system by: improving the sensors' characteristics, reducing the noise of charge amplifier V_{ndop}, reducing the capacitances and the parasitic capacitances of the ASIC and the sensors, increasing the excitation sensor signal amplitudes, *etc.*

Figure S3. Simulated spectrum at the output of the analog front-end. The spectral lines correspond to different sensors: S1: δC_1 = 100 aF, f_{S1} = 8.8 kHz, S2: δC_2 = 50 aF, f_{S2} = 10.9 kHz, S3: δC_3 = 10 aF, f_{S3} = 13.9 kHz, S4: δC_4 = 5 aF, f_{S4} = 16.3 kHz.

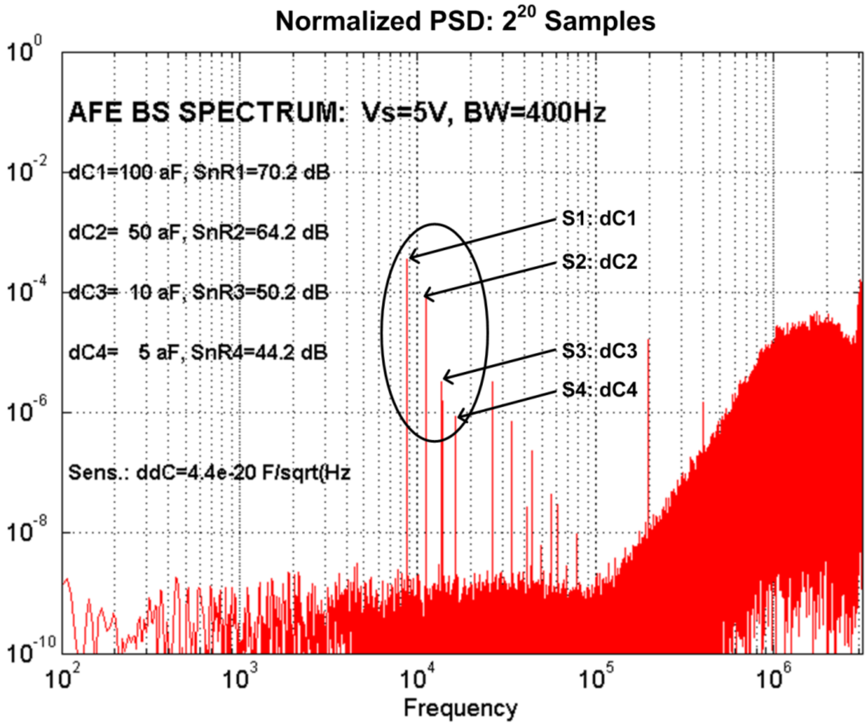

References

1. Siprak, D.; Tiebout, M.; Zanolla, N.; Baumgartner, P. Noise reduction in CMOS circuits through switched gate and forward substrate bias. *IEEE J. Solid-State Circuits* **2009**, *44*, 1959–1967.
2. Park, C.; Seo, H.; Kim, B. A noise optimized passive mixer for charge-domain sampling applications. *J. Electromagn. Waves Appl.* **2009**, *23*, 1909–1917.
3. Tavakoli, M.; Sarpeshkar, R. An offset-canceling low-noise lock-in architecture for capacitive sensing. *IEEE J. Solid-State Circuits* **2003**, *38*, 244–253.
4. Sormaillon, M.O.; Urteaga, R.; Bonetto, F.J. High-frequency digital lock-in amplifier using random sampling. *IEEE Trans. Instrum. Meas.* **2008**, *57*, 616–621.
5. Burns, M.; Roberts, G.W. *An Introduction to Mixed-Signal IC Test and Measurement*; Oxford University Press: Oxford, UK, 2001.
6. Wee, K.H.; Sarpeshkar, R. An electronically tuneable linear or nonlinear MOS resistor. *IEEE Trans. Circuits Syst. I* **2008**, *55*, 2573–2583.
7. Chehrazi, S.; Mirzaei, A.; Abidi, A.A. Noise in current-commutating passive FET mixers. *IEEE Trans. Circuits Syst. I* **2010**, *57*, 332–344.
8. Van der Wel, A.P.; Klumperink, E.A.M.; Kolhatkar, J.S.; Hoekstra, E.; Snoeij, M.F.; Salm, C.; Wallinga, H.; Nauta, B. Low-frequency noise phenomena in switched MOSFETs. *IEEE J. Solid-State Circuits* **2007**, *42*, 540–550.

9. Chen, Y.; Xu, P.C.; Li, X.X. Self-assembling siloxane bilayer directly on SiO_2 surface of micro-cantilevers for long-term, highly repeatable sensing of trace explosives. *Nanotechnology* **2010**, *21*, 1–10.
10. Strle, D. Mixed-signal circuits modeling and simulations using Matlab. In *Engineering Education and Research Using MATLAB*; Assisi, A., Ed.; InTeh: Rijeka, Croatia, 2011; pp. 113–148.
11. Raič, D.; Strle, D. Advanced decimator modelling with HDL conversion in mind. In *MATLAB*; Bennett, K., Ed.; InTeh: Rijeka, Croatia, 2014.